

# Two newly identified eclipsing binaries in open cluster NGC 3532

Özdarcan O.<sup>1,2</sup>★

<sup>1</sup>Ege University, Science Faculty, Department of Astronomy and Space Sciences, 35100 Bornova, İzmir, Turkey

<sup>2</sup>TÜBİTAK National Observatory, Akdeniz University Campus, 07058 Konyaaltı, Antalya, Turkey

Accepted XXX. Received YYY; in original form ZZZ

## ABSTRACT

We present light curve analyses of two newly identified detached eclipsing binaries, HD 96609 and HD 303734, in the region of the richly populated open cluster NGC 3532. HD 96609 is composed of two main sequence stars (B9-A0V + A2V) with masses and radii of  $M_1 = 2.66 \pm 0.02 M_\odot$ ,  $M_2 = 1.84 \pm 0.01 M_\odot$ ,  $R_1 = 2.740 \pm 0.006 R_\odot$ ,  $R_2 = 1.697 \pm 0.005 R_\odot$ . The positions of the components on  $\log M - \log R$  plane suggests  $\log(\text{age/yr})$  8.55, corresponding  $350 \pm 40$  Myr of age, which agrees with the  $300 \pm 100$  Myr age of NGC 3532 estimated in previous studies. We find the distance of HD 96609 as  $460 \pm 17$  pc, which is consistent with the  $484^{+35}_{-30}$  pc distance of NGC 3532, estimated from GAIA parallaxes. HD 303734 is an interesting totally eclipsing binary with a quite shallow secondary eclipse. Using photometric properties of the system in conjunction with theoretical calibrations, we estimate that HD 303734 consists of A6V + K3V components. HD 96609 and HD 303734 are the second and third eclipsing binaries discovered in the region of NGC 3532, after the first one, GV Car.

**Key words:** stars: binaries: eclipsing – stars: binaries: spectroscopic – Galaxy: open clusters and associations: individual: NGC 3532 – stars: individual: HD 96609 – stars: individual: HD 303734

## 1 INTRODUCTION

NGC 3532 is one of the most spectacular and richly populated open cluster located in the southern sky. Although these properties, less number of studies exist on the cluster compared to other well-known southern open clusters. The first comprehensive *UBV* photoelectric photometry of the cluster was presented by Koelbloed (1959), who used the main-sequence fitting method and determined the distance of the cluster as  $432 \pm 40$  pc with an  $E(B - V)$  value of  $0^m01$  and an approximate age of 100 Myr. Subsequent broad-band photometric studies were provided by Fernandez & Salgado (1980), Wizinowich & Garrison (1982) and Claria & Lapasset (1988) with additional DDO and Washington photometry. Moreover, Ström-gren *uvbyH $\beta$*  photometry of the cluster were presented by Eggen (1981) and Schneider (1987). The most recent, comprehensive and precise *BVR* photometry of the cluster, going deeper magnitudes of  $V = 22^m$ , was published by Clem et al. (2011), who revised the distance and  $E(B - V)$  value of the cluster as  $492^{+12}_{-11}$  pc and  $0^m028 \pm 0^m006$ , respectively. They also revised the age of the cluster as  $300 \pm 100$  Myr by using fitting overshooting isochrones to the upper main sequence of the cluster in colour-magnitude diagram. The distance estimation of Clem et al. (2011) matches the most recently reported distance of the cluster,  $484^{+35}_{-30}$  pc, which is computed via parallax measurements included in the second GAIA data release (Fritzewski et al. 2019; Gaia Collaboration et al. 2016,

2018). Recent studies indicate that the cluster possesses near solar metallicity (Bossini et al. 2019; Fritzewski et al. 2019).

Beside photometric studies, González & Lapasset (2002) investigated spectroscopic binaries and kinematic membership in NGC 3532. They discovered SB2 nature of HD 96609, which is also a member of the cluster and one of the main targets in this study. Large radial velocity semi-amplitudes of the components ( $K_1 = 71.23 \pm 0.25$  km s<sup>-1</sup> and  $K_2 = 102.94 \pm 0.32$  km s<sup>-1</sup>) indicate high orbital inclination, i.e. possible eclipsing nature of the system. No eclipse event has been reported for this system so far. However, preliminary inspection of space photometry provided by Transiting Exoplanet Survey Satellite (TESS, Ricker et al. 2014) clearly shows that the system is an eclipsing binary with an approximate orbital period of 8.2 day. Further evidences of eclipses is noticeable in The All Sky Automated Survey (ASAS) photometry (hereafter, ASAS3; Pojmanski 1997, 2002; Pojmanski et al. 2005). Preliminary inspection of TESS photometry of the stars in the field of NGC 3532 reveals one more eclipsing binary star, HD 303734. We show positions of these newly identified eclipsing binaries in colour-magnitude diagram of NGC 3532 in Fig. 1. Both systems are located in the main sequence band of the cluster. Furthermore, we note that HD 96609 is very close to the main sequence turn-off point, thus deserves attention for modelling. In Fig. 1, we also show the position of the first discovered eclipsing binary in the region of NGC 3532, GV Car (Southworth & Clausen 2006). We note that the positions of HD 96609 and GV Car in colour-magnitude diagram, which are very close to each other, is remarkable.

★ E-mail: orkun.ozdarcan@ege.edu.tr

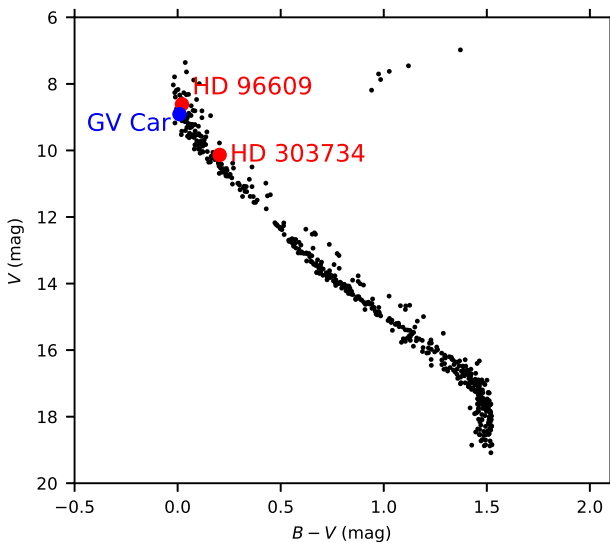


**Figure 1.** Positions of the target systems and GV Car in colour-magnitude diagram of NGC 3532. Photometric data are taken from [Clem et al. \(2011\)](#). Plotted data belong to kinematic members of the cluster given in [Cantat-Gaudin et al. \(2018\)](#).

In this study, we present light curve modelling of newly discovered eclipsing binaries HD 96609 and HD 303734. In the case of HD 96609, we use the advantage of simultaneous analysis of radial velocity and light curve data to compute physical parameters of the system and its age, which could be used to test previous age and distance estimations of NGC 3532. However, due to the lack of spectroscopic data, analysis of HD 303734 are based on pure photometric data. In the next section, we describe the data used in this study, while we give details of light curve and radial velocity modelling in Section 3. In the last section, we summarize and discuss our findings with a comparison between physical properties of our target stars and basic properties of NGC 3532.

## 2 DATA

Radial velocity measurements of HD 96609, which are sufficient in number to reveal orbital motion, were published by [González & Lapasset \(2002\)](#), where radial velocities of both components could be measured. These measurements are based on optical spectra recorded by REOSC échelle spectrograph with a spectral resolution of  $R = \lambda/\Delta\lambda = 13\,300$ . [González & Lapasset \(2002\)](#) reported that the rotational velocities of both components of HD 96609 is below the instrumental error of REOSC spectrograph ( $v \sin i < 20 \text{ km s}^{-1}$ ). They obtained radial velocities by applying two-dimensional cross-correlation method described in [Zucker & Mazeh \(1994\)](#) via TODCOR algorithm. Target star spectra were cross-correlated with spectra of two reference stars (HR 6041 and HR 3321). Strong blending in spectral lines of both components was observed due to the small radial velocity differences ( $v_r < 35 \text{ km s}^{-1}$ ) between the components in the vicinity of eclipse phases. In these cases, rms residuals are larger by factor of 3 and 4.5 for the primary and the secondary components, respectively. More details on radial velocity measurement technique can be found in [González & Lapasset \(2000\)](#). We use these measurements for spectroscopic orbit modelling. However, there is no radial velocity based orbital solution for HD 303734, thus analysis of this system purely relies on photometry.

The main source of photometric data is space photometry provided by TESS mission, where Quick Look Pipeline (QLP) data from sector 10 and 11 observations are available for the target systems. Exposure time of these observations is 30 minutes, which provides pretty good signal-to-noise ratio for basic light curve modelling of our targets. We adopt KSPSAP FLUX measurements ([Huang et al. 2020](#)), which are obtained by de-trending simple aperture photometry (SAP) fluxes. Before de-trending, high-pass filter are applied to the SAP fluxes in order to remove low-frequency variability originating from stellar activity or instrumental noise. After de-trending, fluxes are extracted for three apertures with different sizes. Fluxes obtained from the best aperture, which is 3 pixels in size, are labelled as KSPSAP FLUX. In practice, we obtain KSPSAP FLUX measurements by using LIGHTKURVE package written in PYTHON environment ([Lightcurve Collaboration et al. 2018](#)). In the case of crowded regions, such as star clusters, extracted fluxes of a given target could be contaminated by neighbouring light sources in the close vicinity because of large pixel scale of 21 arc-seconds per pixel for TESS images. However, during extraction of QLP fluxes [Huang et al. \(2020\)](#) applied an efficient background subtraction algorithm which is based on differential photometry of nearby light sources. If the nearby light sources are not varying significantly, then the method is capable of removing large part of the background contamination from nearby light sources inside 3 pixels of aperture. For a given target, if one or more nearby light sources are variable, then the observed light curve amplitude of the main target would be incorrect. Since HD 96609 and HD 303734 are dominantly bright targets in their separately defined apertures, amplitude of possible variability of any background source in the apertures should be negligible, thus we assume zero background contribution to the light curves of the target system.

Eclipsing binary natures of these systems are noticeable in ASAS3 photometry obtained in V bandpass. ASAS3 data of both systems cover 8 years of time span starting from HJD 24 52000 and ending in HJD 24 55000. Observational strategy of ASAS telescopes is to obtain one or a few measurements per observing night from a target area in the sky. Depending on orbital period, application of this strategy for a sufficiently long time may provide good phase coverage of full orbital cycle for an eclipsing binary, including egress, ingress and eclipse phases. We adopt ASAS3 measurements with a quality flag of A or B and check for extreme outlier points in the light curve by eye inspection. We show TESS and ASAS3 photometry versus barycentric (for TESS data) and heliocentric (for ASAS3 data) Julian Date in Fig. 2.

## 3 ANALYSIS

We perform light curve modelling with the v40 version of the FORTRAN code JKTEBOP<sup>1</sup> ([Southworth et al. 2004, 2005](#)), which is mainly based on ECLIPSING BINARY ORBIT PROGRAM (EBOP, [Popper & Etzel 1981](#)) written by Paul Etzel. The program uses biaxial ellipsoidal model ([Nelson & Davis 1972](#)) which is also known as Nelson-Davis-Etzel biaxial ellipsoidal model. The JKTEBOP code is capable of very fast modelling of well-detached eclipsing binaries and equipped with detailed and robust error analysis routines. However, the code is not capable of light curve modelling of very close eclipsing binaries since binarity effects due to the distorted shapes of the components become dominant at out of eclipse phases and

<sup>1</sup> <https://www.astro.keele.ac.uk/jkt/codes/jktebop.html>

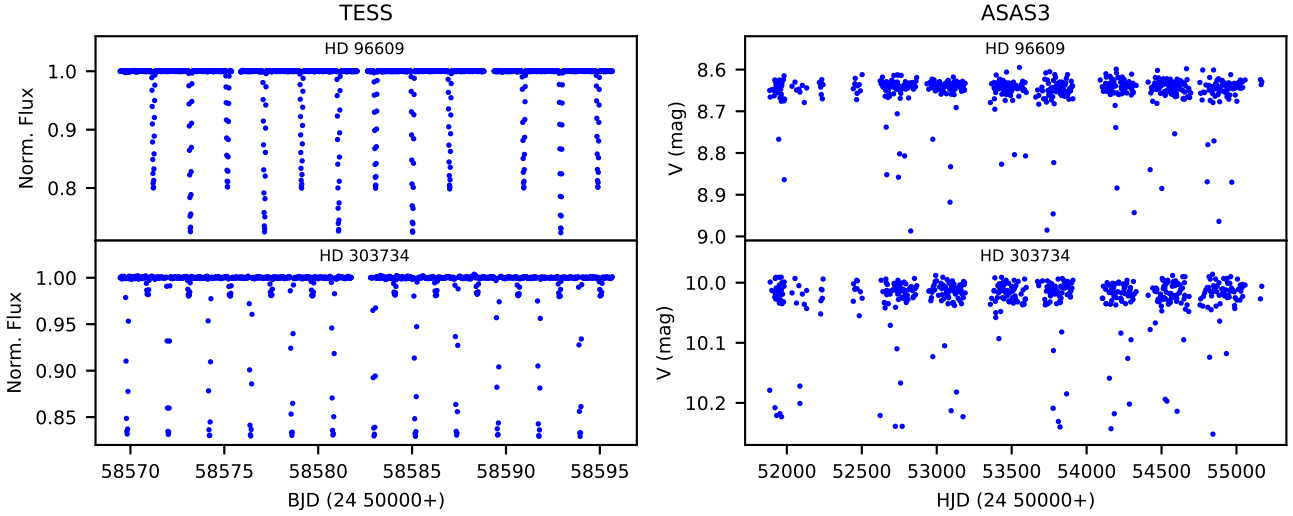


**Figure 2.** TESS and ASAS3 photometry of the target stars.

can not be fitted by Nelson-Davis-Etzel model properly. It is also not possible to model stellar spots and pulsations with the JKTEBOP code.

Inspecting the ASAS3 light curves of HD 96609, we noticed that there are few data points around ingress and egress phases, which may highly reduce the precision of fractional radii resulting from the best-fitting model and lead to erroneous results. We observe quantitative evidence of this possibility in trial-error light curve modelling process before final modelling stage. In preliminary light curve modelling attempts, we observe that resulting fractional radii from the best-fitting models for TESS and ASAS3 light curves do not agree. In the case of HD 96609, more massive star appears as the larger star in the system according to the best-fitting light curve model for TESS data, while modelling results of ASAS3 data indicate that the same star is the smaller one in the system. Furthermore, internal errors of fractional radii are 100 times larger for ASAS3 model results compared to TESS model results. Similar situation is valid for HD 303734. Moreover, secondary eclipse of HD 303734 is not distinguishable in ASAS3 light curves due to observational scatter. Therefore, we exclude ASAS3 data from analyses for both systems.

We have both radial velocity data and high precision TESS photometry for HD 96609, thus we model two data simultaneously. Before modelling, we simply convert normalized TESS fluxes to the magnitudes by using the equation  $m = -2.5 \times \log(F)$ , where  $F$  denotes normalized TESS flux. We adjust mid-time of the primary eclipse ( $T_0$ ), orbital period ( $P$ ), light scale factor ( $S$ ), fractional radii of the larger and smaller components ( $r_1$  and  $r_2$ , respectively), surface brightness ratio ( $J$ ), inclination of the orbital plane ( $i$ ), radial velocity semi-amplitudes of the larger and smaller components ( $K_1$  and  $K_2$ , respectively) and center-of-mass velocity of the system ( $V_\gamma$ ). Besides, depending on  $K_1$  and  $K_2$ , the code internally computes the mass ratio of the system  $q = M_2/M_1$ , where  $M_1$  and  $M_2$  denote the masses of the more massive and less massive components, respectively. Since we do not observe any considerable light variation at out-of eclipse phases, we fix photometric mass ratio value to a negative number in order to force the stars to be spherical. This is a feature of JKTEBOP code. We adopt square root limb darkening law (Diaz-Cordoves & Gimenez 1992) for both components of HD 96609. We use limb darkening coefficients of Claret (2017) which are computed for TESS bandpass by using plane-

parallel ATLAS stellar atmosphere models with solar metallicity and  $2 \text{ km s}^{-1}$  of micro-turbulence velocity. We consider effective temperature and surface gravity of each component in order to determine linear ( $x$ ) and non-linear ( $y$ ) limb darkening coefficients by applying linear interpolation in the tables of Claret (2017). We do not adjust limb darkening coefficients during analyses. Since the model is well constrained by radial velocity data and high precision TESS photometry, model convergence is very fast for HD 96609.

We have TESS photometry but no radial velocity data for HD 303734. Thus, we only adjust  $T_0$ ,  $P$ ,  $S$ ,  $r_1$ ,  $r_2$ ,  $J$  and  $i$  during light curve modelling of this system. Ignoring radial velocity data and related adjustable parameters, applied modelling strategy is the same as in the case of HD 96609. We use square root and linear limb darkening laws for the primary and the secondary components, respectively, and we follow the reference and strategy mentioned above for determination of limb darkening coefficients.

We show phase-folded observations and the best-fitting models in Fig. 3 and 4 for HD 96609 and HD 303734, respectively. We note that we show ASAS3 data only for comparison purposes in these figures. Although the best-fitting models for observational data of each system appear fairly good in these figures, we discuss stability of the best-fitting model for HD 303734 in later paragraphs.

One may obtain formal uncertainties of final model parameters from solution covariance matrix. JKTEBOP code provides these uncertainties at the end of each solution run. However, these uncertainties are mostly underestimated or unrealistically small due to the possible strong correlations between adjusted parameters. In order to compute more realistic uncertainties, we use TASK8 feature of the JKTEBOP, which applies Monte Carlo simulations. In application of TASK8 for each target, the code re-evaluates the best-fitting model at the phases of the actual observations by adding Gaussian noise. We set the code to repeat this process for 10 000 times and compute a set of solution parameters for each process. Finally, we compute standard deviation of the 10 000 different results of each adjustable parameter and adopt this standard deviation as the final uncertainty of the corresponding adjusted parameter. We tabulate final best-fitting model parameters and  $1\sigma$  uncertainties estimated from Monte Carlo simulations in Table 1. We note that the lack of radial velocity observations between 1.1 and 1.4 phases might probably responsible for a significant amount of the uncertainties tabulated for  $K_1$  and  $K_2$  parameters in the table. We also show dis-

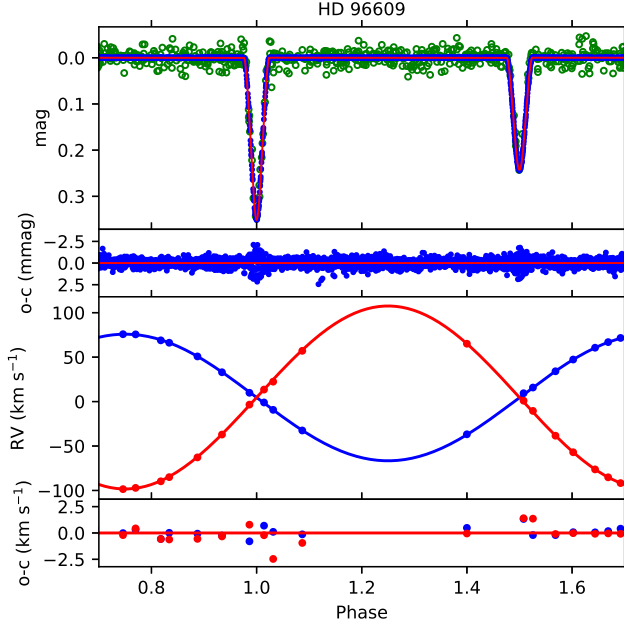


**Figure 3.** TESS photometry (blue points), radial velocity measurements (blue and red points for the more massive and less massive components, respectively) and the best-fitting light curve and spectroscopic orbit models of HD 96609 (continuous curves). We also over plot ASAS3 photometry (green open circles) for comparison. Note that we apply constant shift of  $8^{\text{m}}64$  to ASAS3 magnitudes in order to evaluate TESS and ASAS3 data in a common scale.

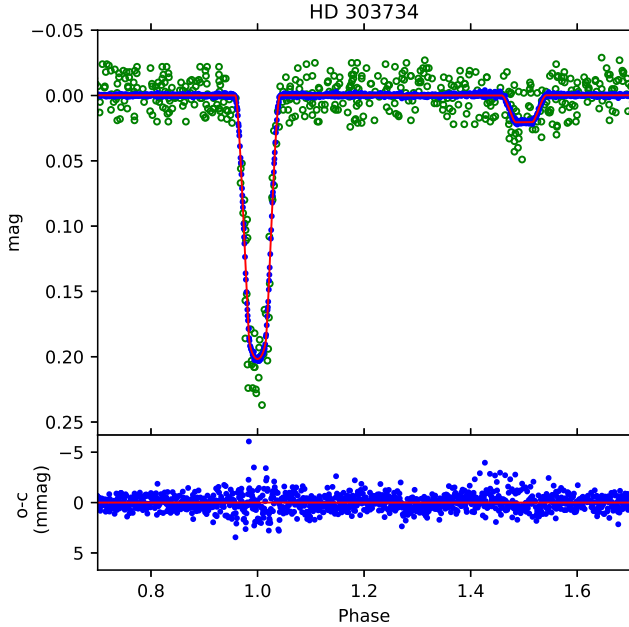


**Figure 4.** TESS photometry (blue points) and the best-fitting light curve model of HD 303734 (continuous curve). ASAS3 photometry is shown by green open circles for comparison. Note that we apply constant shift of  $10^{\text{m}}015$  to ASAS3 magnitudes in order to evaluate TESS and ASAS3 data in a common scale.

**Table 1.** JKTEBOP modelling results of the target stars. In the lower part of the table, we tabulate computed absolute parameters of HD 96609.

Model Parameters	HD 96609	HD 303734
$T_0$ (BJD)	58577.22101 (2)	58569.82053 (5)
$P$ (day)	8.191924 (3)	2.193648 (9)
$S$ (mag)	-0.000040 (8)	-0.00016 (2)
$J$	0.7414 (3)	0.1329 (7)
$x_1, y_1$	-0.038, 0.553	-0.072, 0.668
$x_2, y_2$	-0.027, 0.561	0.559, —
$r_1$	0.09703 (4)	0.1896 (2)
$r_2$	0.00010 (12)	0.0754 (1)
$i$ ( $^\circ$ )	87.02 (1)	86.48 (4)
$K_1$ (km s $^{-1}$ )	71.2 (3)	—
$K_2$ (km s $^{-1}$ )	102.9 (3)	—
$V_\gamma$ (km s $^{-1}$ )	4.6 (1)	—
$e$	0	0
$\omega$ ( $^\circ$ )	—	—
$q = M_2/M_1$	0.692 (4)	—
lc rms (mmag)	0.455	0.834
$r v_1$ rms (km s $^{-1}$ )	0.46	—
$r v_2$ rms (km s $^{-1}$ )	0.84	—
Physical Parameters		
$a$ ( $R_\odot$ )	28.23 (6)	—
$M_1$ ( $M_\odot$ )	2.66 (2)	—
$M_2$ ( $M_\odot$ )	1.84 (1)	—
$R_1$ ( $R_\odot$ )	2.740 (6)	—
$R_2$ ( $R_\odot$ )	1.697 (5)	—
$\log g_1$ (cgs)	3.987 (1)	—
$\log g_2$ (cgs)	4.243 (2)	—
$T_1$ (K)	9650 (250)	7970 (500)
$T_2$ (K)	8950 (250)	4812 (300)
$\log L_1$ ( $L_\odot$ )	1.76 (4)	—
$\log L_2$ ( $L_\odot$ )	1.22 (4)	—
$M_{\text{Bol}1}$ (mag)	0.32 (11)	—
$M_{\text{Bol}2}$ (mag)	1.69 (12)	—
$d$ (pc)	460 (17)	—

tribution of Monte Carlo simulations for each target in Fig. 5 and 6, in order to illustrate correlations between adjusted parameters.

Inspecting Fig. 5, we do not see any remarkable skewness in correlation plots, which is clearly the result of good parameter constraints provided by simultaneous modelling of light curve and radial velocity data. On the other hand, model parameter constraint is not very good due to the absence of spectroscopic data in the case of HD 303734. Slight skewness in correlation plots of some parameters may easily be noticed in Fig. 6. However, we are still able to obtain reasonable representation of TESS light curve of HD 303734.

Since JKTEBOP does not work with effective temperatures, we can not directly include effective temperatures in modelling process. However, we may use photometric data of HD 96609 as an auxiliary property and estimate the effective temperatures, which enables us to compute the distance of the system. Adopting  $E(B-V) = 0^{\text{m}}028$  and  $B-V = 0^{\text{m}}021 \pm 0^{\text{m}}010$  from Clem et al. (2011), we find  $(B-V)_0 = -0^{\text{m}}007 \pm 0^{\text{m}}010$  corresponding to an effective temperature of 9650 K and spectral type of B9-A0V according to the calibrations given by Gray (2005). Uncertainty of  $B-V$  colour indicates 120 K of uncertainty on the effective temperature according to this calibration. However, 120 K of uncertainty estimated from broad band photometry is probably underestimated for such a hot star, thus we believe that the real uncertainty is higher and

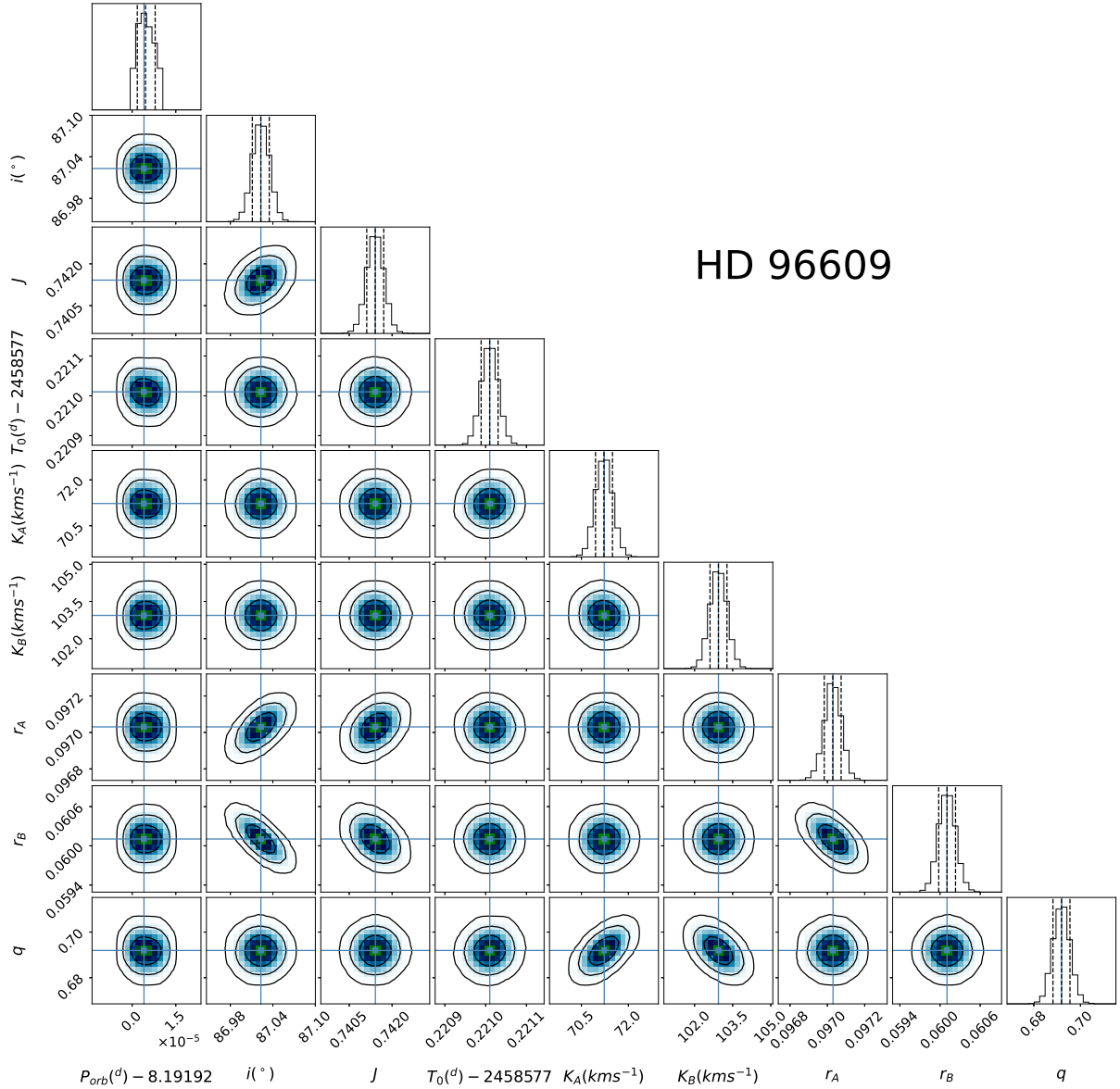


**Figure 5.** Distribution of results from 10 000 Monte Carlo simulations for HD 96609. The figure is made by using `corner.py` script (Foreman-Mackey 2016). Three contour levels in each plot window show 1, 2 and 3  $\sigma$  levels. Diagonal histogram plots show posterior distribution of each parameter.

approximately around 250 K. Assuming that the resulting surface brightness ratio  $J$  in Table 1 could be considered as approximate ratio of the effective temperatures in terms of  $(T_2/T_1)^4$ , we compute the effective temperature of the secondary component as 8950 K, corresponding to A2V spectral type. Although  $J$  is computed via photometric data obtained in TESS bandpass, it is still fairly reasonable to assume that  $J \approx (T_2/T_1)^4$  since temperature difference between the primary and the secondary component is not large. Feeding these values, adopted  $V$  magnitude and  $E(B - V)$  values of HD 96609 from Clem et al. (2011) together with  $P$ ,  $K_1$ ,  $K_2$ ,  $i$ ,  $r_1$ ,  $r_2$ ,  $T_1$  and  $T_2$  into the JKTABSDIM<sup>2</sup> code, we obtain absolute physical properties and the distance of HD 96609. JKTABSDIM

code computes absolute bolometric magnitudes of the components by assuming  $T_{eff} = 5780$  K and  $M_{bol} = 4^m.74$  as solar values. Considering various calibrations (Bessell et al. 1998; Girardi et al. 2002; Code et al. 1976; Flower 1996; Kervella et al. 2004) the code applies bolometric correction in  $V$  band to the computed absolute bolometric magnitudes, which ultimately provides absolute  $V$  magnitudes of the components separately, overall absolute  $V$  magnitude of the system and finally the distance of the system for each calibration separately. Averaging distance values from calibrations referred above, we finally compute the average distance of the system. We tabulate all results in the second column of Table 1.

Light curve modelling of HD 303734 reveals that the system is a totally eclipsing binary. Although lack of radial velocity data prevents us from computing precise physical parameters, we may use photometric properties of the system to reveal its nature a little

<sup>2</sup> <https://www.astro.keele.ac.uk/jkt/codes/jktabsdim.html>



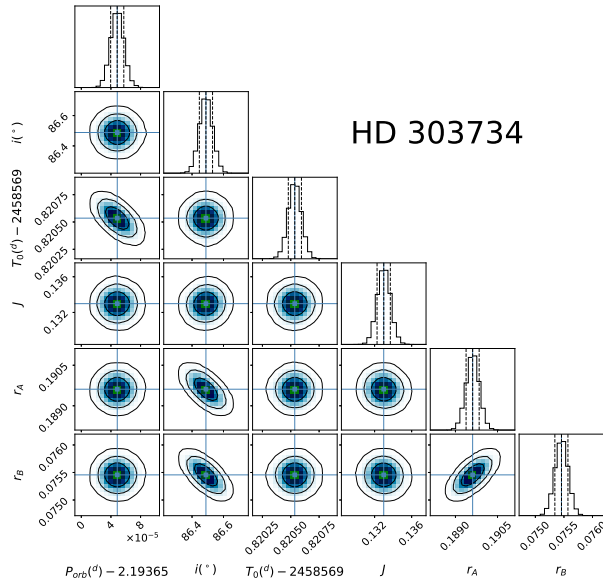


**Figure 6.** Distribution of results from 10000 Monte Carlo simulations for HD 303734.

more. Following the same method proposed for HD 96609 above and adopting same calibrations, we find  $(B - V)_0 = 0^m176 \pm 0^m041$  corresponding to an average effective temperature of  $7970 \pm 500$  K and spectral type of A6V. Main source of larger uncertainty compared to the case of HD 96609 is the  $\sim 6$  times larger uncertainty on  $V$  measurement ( $V = 10^m135 \pm 0^m040$ , Clem et al. 2011) compared to the  $V$  measurement of HD 96609. Surface brightness ratio of the components found in the light curve modelling suggests 4812 K for the effective temperature of the secondary component, indicating K3V spectral type. Large temperature difference between the components of HD 303734 is remarkable. In this case, effective temperature estimation of the secondary component via  $J \approx (T_2/T_1)^4$  approximation can not be very precise because the surface brightness ratio depends on not only the ratio of the temperatures but also the bandpass used in the photometry. In the case of HD 303734, components of the system appear to possess different spectral energy distribution, thus  $J$  would be very likely different in different specific wavelength ranges (i.e. bandpasses). Therefore, estimated 4812 K effective temperature of the secondary component should be considered with caution. Due to the lack of spectroscopic orbit solution, we refrain from further evaluation of the system since indirect estimations of physical properties would include very large uncertainties.

#### 4 DISCUSSION

Simultaneous light curve and spectroscopic orbit modelling of HD 96609 enables us to compute precise masses and radii of the components. We plot components of HD 96609 on  $\log M - \log R$  plane in upper panel of Fig. 7 together with Precomputed Padova and Trieste Stellar Evolution Code (PARSEC) isochrones Bressan et al. (2012) for solar metallicity with  $Y = 0.279$  and  $Z = 0.017$ . Inspecting positions of the components, we find that the best-fitting isochrone has  $\log(\text{age}/\text{yr})$  8.55. Considering uncertainty of masses in the figure and plotted isochrones, we estimate the age of the system as  $350 \pm 40$  Myr, which nicely agrees with the  $300 \pm 100$

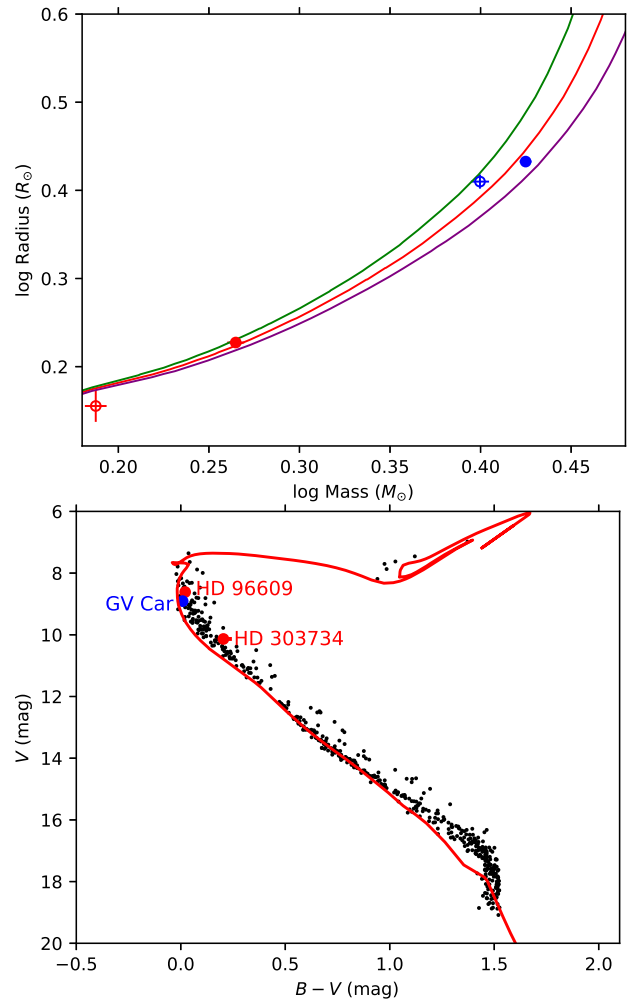


**Figure 7.** Upper panel: Positions of the components of HD 96609 on  $\log M - \log R$  plane (filled circles). Both components of GV Car are also plotted in the panel with open circles. Plotted isochrones are for  $\log(\text{age}/\text{yr})$  8.5 (purple), 8.55 (red) and 8.6 (green). Note that error bars are mostly smaller than the size of filled circles for the components for HD 96609. Lower panel: Same as Figure 1 but with  $\log(\text{age}/\text{yr})$  8.55 isochrone over plotted.

Myr age estimation of Clem et al. (2011). In the figure, we also over plot the components of the detached eclipsing binary GV Car, which is also the member of the cluster and the first eclipsing binary discovered in NGC 3532 (Southworth & Clausen 2006). Position of the primary component of GV Car is consistent with the isochrone of  $\log(\text{age}/\text{yr})$  8.55 but the secondary component appears outside of the plotted isochrones, even if we consider the  $1\sigma$  error bars. Eclipse depth variation of GV Car was reported in the same study and two possible explanations suggested for this variation. There is either a decrease in the orbital inclination by  $3^\circ$  due to a perturbed orbit or an increase in brightness of a possible third light. Thus, the positional inconsistency of the secondary component of GV Car in Fig. 7 might partly be related to this yet fully unexplained nature of the system. Over plotting  $\log(\text{age}/\text{yr})$  8.55 isochrone in colour-magnitude diagram of the cluster (lower panel of Fig. 7), we see reasonable agreement with the observed data, which supports  $350 \pm 40$  Myr of age. Isochrones plotted in Fig. 7 also confirm that the cluster possesses near solar metallicity.

Computed  $460 \pm 17$  pc distance of HD 96609 in this study

agrees with the  $484^{+35}_{-30}$  pc distance computed from GAIA parallaxes within  $1\sigma$  error. However, considering  $1\sigma$  error, our distance estimation does not agree with the  $492^{+12}_{-11}$  pc distance given by Clem et al. (2011). Comparing three distance estimations, one may note that the distance estimation of Clem et al. (2011) is quite close to the distance estimation based on GAIA parallaxes, while the distance we compute is lower than those estimates. Here, we note that our distance estimation is very sensitive to our effective temperature estimation for the primary component, which is based on de-reddened  $B - V$  colour, and the secondary component, which is computed via surface brightness ratio found from the light curve modelling. Further spectroscopy of the system may help to confirm or improve effective temperature estimations, thus the distance of the system. On the other hand, it is put forwarded that there are strong indications that GAIA parallaxes are affected from a small bias and these parallaxes should be smaller (Lindgren et al. 2021; Groenewegen 2021). This might partly explain the difference between computed distance in this study and the estimated distance of the cluster based on GAIA parallaxes.

We are only able to reveal basic light curve model properties of HD 303734 without its physical properties. Best-fitting light curve model and photometric properties of the system indicate that HD 303734 is a totally eclipsing binary composed of a hot primary component possessing A6V spectral type (w.r.t its estimated effective temperature, Gray 2005) and very cool (likely K3V spectral type) secondary component. Modelling results suggest that both components of the system are main sequence stars. However, model parameter constraint is not as good as in the case of HD 96609. Future optical spectroscopic observations of this system may provide further constraints for a more precise model and test for our findings in this study. Then, it would be possible to evaluate this system as additional reference for further tests on the age and the distance of NGC 3532.

## ACKNOWLEDGEMENTS

I express my thanks to Barış Hoyman for his help on production of some figures in this study. I would like to thank anonymous referee for his/her thoughtful comments and critically reading, which improve and clarify the manuscript. This paper includes data collected by the TESS mission, which are publicly available from the Mikulski Archive for Space Telescopes (MAST). Funding for the TESS mission is provided by the NASA's Science Mission Directorate. This research has made use of NASA's Astrophysics Data System. This research has made use of the SIMBAD database, operated at CDS, Strasbourg, France.

*Software:* PYTHON, NUMPY (Harris et al. 2020), MATPLOTLIB (Hunter 2007), SCIPY (Virtanen et al. 2020).

## DATA AVAILABILITY

ASAS V-band photometric data of HD 96609 available from [http://www.astrouw.edu.pl/cgi-asas/asas.cgi\\_get\\_data?110327-5829.8,asas3](http://www.astrouw.edu.pl/cgi-asas/asas.cgi_get_data?110327-5829.8,asas3). ASAS V-band photometric data of HD 303734 available from [http://www.astrouw.edu.pl/cgi-asas/asas.cgi\\_get\\_data?110651-5842.4,asas3](http://www.astrouw.edu.pl/cgi-asas/asas.cgi_get_data?110651-5842.4,asas3). The TESS QLP data used in this paper are available on MAST.

## REFERENCES

- Bessell M. S., Castelli F., Plez B., 1998, *A&A*, **333**, 231  
 Bossini D., et al., 2019, *A&A*, **623**, A108  
 Bressan A., Marigo P., Girardi L., Salasnich B., Dal Cero C., Rubele S., Nanni A., 2012, *MNRAS*, **427**, 127  
 Cantat-Gaudin T., et al., 2018, *A&A*, **618**, A93  
 Claret A., 2017, *A&A*, **600**, A30  
 Claria J. J., Lapasset E., 1988, *MNRAS*, **235**, 1129  
 Clem J. L., Landolt A. U., Hoard D. W., Wachter S., 2011, *AJ*, **141**, 115  
 Code A. D., Bressan R. C., Davis J., Brown R. H., 1976, *ApJ*, **203**, 417  
 Diaz-Cordoves J., Gimenez A., 1992, *A&A*, **259**, 227  
 Eggen O. J., 1981, *ApJ*, **246**, 817  
 Fernandez J. A., Salgado C. W., 1980, *A&AS*, **39**, 11  
 Flower P. J., 1996, *ApJ*, **469**, 355  
 Foreman-Mackey D., 2016, *The Journal of Open Source Software*, **1**, 24  
 Fritzewski D. J., Barnes S. A., James D. J., Geller A. M., Meibom S., Strassmeier K. G., 2019, *A&A*, **622**, A110  
 Gaia Collaboration et al., 2016, *A&A*, **595**, A1  
 Gaia Collaboration et al., 2018, *A&A*, **616**, A1  
 Girardi L., Bertelli G., Bressan A., Chiosi C., Groenewegen M. A. T., Marigo P., Salasnich B., Weiss A., 2002, *A&A*, **391**, 195  
 González J. F., Lapasset E., 2000, *AJ*, **119**, 2296  
 González J. F., Lapasset E., 2002, *AJ*, **123**, 3318  
 Gray D. F., 2005, *The Observation and Analysis of Stellar Photospheres*, 3 edn. Cambridge University Press, doi:10.1017/CBO9781316036570  
 Groenewegen M., 2021, arXiv e-prints, p. arXiv:2106.08128  
 Harris C. R., et al., 2020, *Nature*, **585**, 357  
 Huang C. X., et al., 2020, *Research Notes of the American Astronomical Society*, **4**, 206  
 Hunter J. D., 2007, *Computing in Science & Engineering*, **9**, 90  
 Kervella P., Thévenin F., Di Folco E., Ségransan D., 2004, *A&A*, **426**, 297  
 Koelbloed D., 1959, *Bull. Astron. Inst. Netherlands*, **14**, 265  
 Lightkurve Collaboration et al., 2018, *Lightkurve: Kepler and TESS time series analysis in Python*, *Astrophysics Source Code Library* (ascl:1812.013)  
 Lindgren L., et al., 2021, *A&A*, **649**, A4  
 Nelson B., Davis W. D., 1972, *ApJ*, **174**, 617  
 Pojmanski G., 1997, *Acta Astron.*, **47**, 467  
 Pojmanski G., 2002, *Acta Astron.*, **52**, 397  
 Pojmanski G., Pilecki B., Szczygiel D., 2005, *Acta Astron.*, **55**, 275  
 Popper D. M., Etzel P. B., 1981, *AJ*, **86**, 102  
 Ricker G. R., et al., 2014, *Journal of Astronomical Telescopes, Instruments, and Systems*, **1**, 1  
 Schneider H., 1987, *A&AS*, **71**, 147  
 Southworth J., Clausen J. V., 2006, *Ap&SS*, **304**, 199  
 Southworth J., Maxted P. F. L., Smalley B., 2004, *MNRAS*, **351**, 1277  
 Southworth J., Maxted P. F. L., Smalley B., 2005, *A&A*, **429**, 645  
 Virtanen P., et al., 2020, *Nature Methods*, **17**, 261  
 Wizinowich P., Garrison R. F., 1982, *AJ*, **87**, 1390  
 Zucker S., Mazeh T., 1994, *ApJ*, **420**, 806

This paper has been typeset from a  $\text{\LaTeX}$  file prepared by the author.